Heatline and Entropy generation analysis of natural convection in a complex enclosure

Rujda Parveen and Tapas Ray Mahapatra
Department of Mathematics, Visva-Bharati (A Central University),
Santiniketan - 731 235, West-Bengal, India.

Abstract

Numerical study of heat transfer characteristics due to steady laminar natural convection within an enclosure with curved (concave/convex) upper wall has been investigated. The bottom wall is considered to be uniformly heated, while the two side walls are linearly heated and the upper curved wall is adiabatic. The test has been performed for wide range of governing parameters like Prandtl number ($Pr = 0.7$ and 1000), Rayleigh number ($10^3 \leq Ra \leq 10^5$) and various concavity and convexity of the upper wall in order to examine the heat transfer and change in motion of fluid flow within the enclosure. Numerical simulations are presented in terms of isotherms (θ), streamlines (ψ), entropy generation due to heat transfer (S_θ), entropy generation due to fluid friction (S_ψ), heatlines (Π), average Nusselt number ($\overline{Nu}$) and average Bejan number (Be_{avg}). The present study shows that the change in curvature of the upper wall affects the thermal behaviour of the fluid inside the enclosure. It is observed that the heat transfer rate in highly convex domain is more as compared to concave domains.

Keywords: Natural convection flow; Complex enclosure; Entropy generation; Heatline; Nusselt number.

Nomenclature

$x,\ y$	:	distance along x and y coordinate
$X,\ Y$	:	dimensionless distance along x and y coordinate
$u,\ v$	:	x and y component of velocity
$U,\ V$	:	x and y component of dimensionless velocity
T, T_0	:	temperature of the fluid and bulk temperature, K
$T_h,\ T_c$	:	temperature of hot and cold wall,
p	:	pressure, Pa
P	:	dimensionless pressure
L	:	length of the enclosure, m
Be_{avg}	:	average Bejan number
g	:	acceleration due to gravity, ms^{-2}
k	:	thermal conductivity,$Wm^{-1}K^{-1}$
n	:	normal vector to the plane
Nu, $\overline{Nu}$	:	local and average Nusselt number
Pr	:	Prandtl number
Ra	:	Rayleigh number
S_θ	:	dimensionless entropy generation due to heat transfer
S_ψ	:	dimensionless entropy generation due to fluid friction
S_{total}	:	dimensionless total entropy generation

Greek symbols

ν	:	kinematic viscosity, m^2s^{-1}
ρ	:	density, kg m^{-3}
θ	:	dimensionless temperature
ϕ	:	irreversibility distribution ratio
α	:	thermal diffusivity, m^2s^{-1}
β	:	volume expansion coefficient, K^{-1}
μ	:	dynamic viscosity, kg $m^{-1}s^{-1}$
Π	:	dimensionless heat function
ψ	:	dimensionless stream function
ξ	:	horizontal coordinate in square

η	:	vertical coordinate in square

Subscripts

l	:	left wall
r	:	right wall
b	:	bottom wall
max	:	maximum
avg	:	average

1 Introduction

Natural Convection in an enclosure or closed cavities has been studied predominantly due to its substantial attention in nature and energy related applications such as solar collector, cooling of electronic components, geothermal energy system, designing of building, food processing etc.

Several investigation on natural convection had been conducted on enclosures with regular geometries (square, rectangular, triangular, trapezoidal etc.) as the thermal characteristics are less complex than the irregular enclosures. Davis [1] studied the natural convection in a square cavity with differentially heated side walls. Basak et al. [3] investigated the natural convection in a square cavity with uniformly and non uniformly heated bottom wall. He observed that the heat transfer is greater in case of non uniform heating as compared to uniform heating case. Kimura and Bejan [4] provided a heatline visualization method for heat transfer in a square cavity. Saha and Khan [5] performed a review study on the natural convection heat transfer in an attic-shaped space. Natural convection in enclosure having triangular shapes has been studied by Kent et al. [6,7]. Several studies have also been performed for rectangular enclosure. Aydin et al. [8] numerically analyzed the natural convection in rectangular enclosure heated from one side and cooled from the ceiling and investigated the effect of Rayleigh number and aspect ratio on heat transfer. Ilis et al. [9] presented the effect of aspect ratio on entropy generation in rectangular cavities having same area. It is found that the total entropy generation due to fluid friction and total entropy generation increase with increasing aspect ratio. Researchers have also carried out natural convection in trapezoidal enclosures. Moukalled and Darwish [10] investigated the effects of the height and position of the baffle mounted on the upper inclined surface of a trapezoidal enclosure. It was found that the overall heat transfer rate is highly effected by the presence of the baffle. Ramakrishna et al. [11] have studied entropy generation and heatlines for free convection in a trapezoidal cavity where left wall is hot and right wall is maintained at constant cold temperature while the horizontal walls are adiabatic. Basak et al. [12] numerically investigated the entropy generation minimization during natural convection in trapezoidal enclosures with various inclination angles for uniformly heated bottom wall, adiabatic top wall with linearly heated side walls (case1) or linearly heated left wall and cold right wall (case2). Anandalakshmi and Basak [13] carried out the entropy distribution and thermal mixing in the steady laminar natural convective flow through the rhombic enclosures with various inclination angles.

Studies dealing with convection problems inside complicated geometries are limited because of complexity of flow inside enclosure which significantly affects the thermal behavior of the fluid inside it. Application of such curved and wavy enclosures is often used in solar energy system, electric machinery, microelectronic industries etc. Morsi and Das [14] numerically found the heat transfer characteristics and flow patterns for complex enclosure. Natural convection in a horizontally wavy enclosure was analyzed by Abdelkader et al. [15]. Varol and oztop [16] conducted expriment to find the effects of aspect ratio on the natural convection heat transfer in a tilted solar collector having absorber on the wavy bottom surface. They observed that the aspect ratio is an effective parameter which can be used to control the heat transfer inside the collector. Das and Mahmud [17] numerically investigated thermal behaviour of fluid inside an enclosure consisting of horizontal wavy wall and vertical straight wall. They obtained that when the amplitude-wavelength ratio changes from zero to other values at lower Grashoff number, heat transfer rate rises. Mahmud and Islam [18] carried out laminar natural convection and entropy generation inside an inclined wavy enclosure. They indicated that, lower the surface waviness, higher is the heat transfer for a particular angular position. Dalal and Das [19,20] have considered a case of natural convection in a cavity with a right wavy vertical wall. They obtained that the presence of undulation in the right wall effects the flow field, thermal field and heat transfer. Adjlout et al. [21] studied the effect of a hot wavy wall due to laminar natural convection in a differentially heated inclined square cavity for different undulations. The study of natural convection inside a wavy cavity filled with fluid saturated porous medium has been numerically examined by Misirlioglu et al. [22]. Biswal and Basak [23,24] made a work on natural convection within differentially heated enclosures with curved (concave/convex) side walls via entropy generation analysis and Bejan's heatline. Due to various related applications of complex enclosures, the study of natural convection in cavities with curved wall may be important to achieve higher heat transfer rate.

Based on the above wide literature survey, it is found that study of heat transfer characteristics in complex geometries is essential in order to obtain the optimal design of the container for various industrial applications. The main interest of this investigation is to study the effect of change in amplitude in the distribution of heat and fluid flow due to natural convection inside an enclosure of top adiabatic curved wall, linearly heated side walls and uniformly heated bottom wall. Numerical estimation will be carried out for different parameters such as Rayleigh number (Ra=$10^3 - 10^5$), Prandtl number (Pr= 0.7 (water) and 1000 (olive/engine oil)) and amplitude of the upper wall (h). Results will be presented in terms of isotherms (θ), streamlines (ψ), entropy generation due to heat transfer (S_θ), entropy generation due to fluid friction (S_ψ) and heatlines (Π). Further more, the effect of Ra and h on average Bejan number and average Nusselt number are also presented. In the current study, the Bi-Conjugate Gradient Stabilized method (BiCGStab) has been employed to solve the non-linear coupled partial differential equations.

2 Physical model

The geometry of the problem considered here is a modified square enclosure of length L with convex or concave upper wall whose amplitude is H. The dimensionless function F(X) which represents the shape of the upper wall of the enclosure is given by

$$F(X) = 1 + hsin(\pi X)$$

where h (=H/L) is the amplitude of the upper wall. When h is positive, upper wall is concave but when h is negative, upper wall is convex. Fig. 1 shows the physical domain of differentially heated enclosure with concave (a) and convex (c) top wall and computational domain (b).

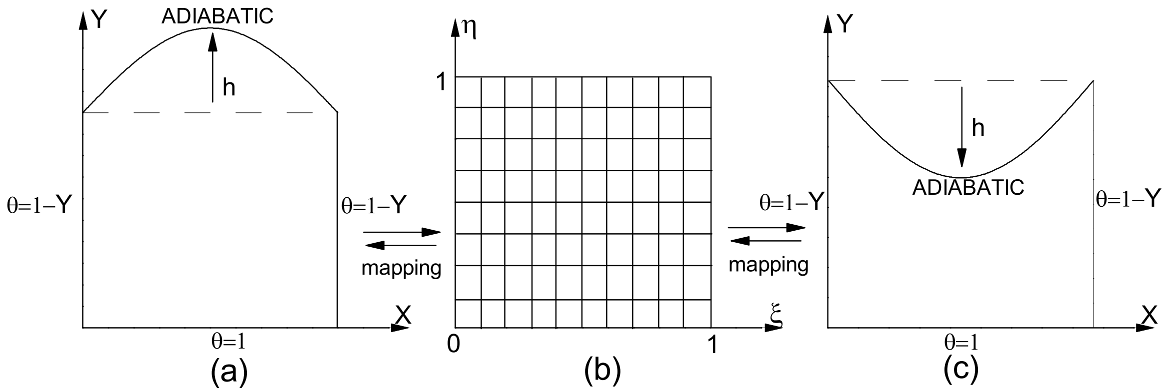

Fig. 1: Schematic diagram of the physical domain (a,c) and computational domain (b).

The left and right walls are linearly heated, the bottom wall is uniformly heated and the top curved wall is kept adiabatic. It is assumed that the fluid is incompressible and Newtonian and the flow is steady and laminar. The boundary conditions for velocity are considered as no slip at the solid boundaries.

3 Mathematical formulations

3.1 *Governing equations*

The dimensionless governing equations for steady natural convection flow are equations representing conservation of mass, momentum and energy and are presented below :

$$\frac{\partial U}{\partial X} + \frac{\partial V}{\partial Y} = 0 \tag{1}$$

$$U\frac{\partial U}{\partial X} + V\frac{\partial U}{\partial Y} = -\frac{\partial P}{\partial X} + Pr\left[\frac{\partial^2 U}{\partial X^2} + \frac{\partial^2 U}{\partial Y^2}\right] \tag{2}$$

$$U\frac{\partial V}{\partial X} + V\frac{\partial V}{\partial Y} = -\frac{\partial P}{\partial Y} + Pr\left[\frac{\partial^2 V}{\partial X^2} + \frac{\partial^2 V}{\partial Y^2}\right] + RaPr\theta \tag{3}$$

$$U\frac{\partial \theta}{\partial X} + V\frac{\partial \theta}{\partial Y} = \left[\frac{\partial^2 \theta}{\partial X^2} + \frac{\partial^2 \theta}{\partial Y^2}\right] \tag{4}$$

where X and Y are dimensionless coordinates along horizontal and vertical directions respectively, U and V are dimensionless velocity components in X and Y directions respectively, P is the dimensionless pressure, θ is the dimensionless temperature, Ra and Pr are the Rayleigh number and Prandtl number respectively.

The dimensionless parameters in the above equations are defined as follows

$$X = \frac{x}{L},\ Y = \frac{y}{L},\ U = \frac{uL}{\alpha},\ V = \frac{vL}{\alpha},\ P = \frac{pL^2}{\rho\alpha^2},$$
$$\theta = \frac{T - T_c}{T_h - T_c},\ Pr = \frac{\nu}{\alpha},\ Ra = \frac{g\beta(T_h - T_c)L^3}{\nu\alpha}$$

where x and y are distances along the horizontal and vertical directions respectively, u and v are the velocity components in the x and y directions respectively, $\alpha, \beta, \nu, \rho, g, T_h, T_c$ are thermal diffusivity, coefficient of volumetric expansion, kinematic viscosity, density of the fluid, gravitational acceleration, temperature of the bottom wall and temperature of top-left / top-right corner, respectively. Stream function (ψ) and vorticity (ω) are defined as

$$U = \frac{\partial \psi}{\partial Y},\quad V = -\frac{\partial \psi}{\partial X},\quad \omega = \frac{\partial V}{\partial X} - \frac{\partial U}{\partial Y}. \tag{5}$$

The anticlockwise circulation is denoted by positive sign and clockwise circulation is represented by negative sign.

3.2 *Boundary conditions*

The corresponding dimensionless boundary conditions for the present problem are specified as follows: All walls, $U = 0,\ V = 0,\ \psi = 0$

At bottom wall, $\theta = 1$

At left and right vertical walls, $\theta = 1 - Y$

At top curved wall, $\frac{\partial \theta}{\partial Y} = 0$

3.3 *Nusselt number*

The Nusselt number, Nu is the measure of convective heat transfer coefficient at the hot surface. Higher the value of Nu, higher is the heat transfer rate from the surface.

The local Nusselt number is computed as

$$Nu = -\frac{\partial \theta}{\partial n},$$

where n is the direction of normal to the plane.
The local Nusselt number along the left wall (Nu_l), right wall (Nu_r) and bottom wall (Nu_b) are defined as follows,

$$Nu_l = \frac{\partial \theta}{\partial X}, \quad Nu_r = -\frac{\partial \theta}{\partial X}, \quad Nu_b = \frac{\partial \theta}{\partial Y}$$

The average Nusselt number is obtained by integrating the local Nusselt number along the respective wall. The average Nusselt number along left wall, right wall and bottom wall are given by

$$\overline{Nu_l} = \int_0^1 Nu_l dX, \quad \overline{Nu_r} = \int_0^1 Nu_r dX, \quad \overline{Nu_b} = \int_0^1 Nu_b dY. \tag{6}$$

To evaluate eq. (6), a Simpson's $\frac{1}{3}$rd rule of integration is implemented.

3.4 *Entropy generation*

According to local thermodynamic equilibrium of the linear transport theory, the dimensionless local entropy generation due to heat transfer (S_θ) and due to fluid friction (S_ψ) for a two dimensional heat and fluid flow in the cartesian coordinate can be written as

$$\begin{aligned} S_\theta &= \left(\frac{\partial \theta}{\partial X}\right)^2 + \left(\frac{\partial \theta}{\partial Y}\right)^2, \\ S_\psi &= \phi \left[2 \left(\left(\frac{\partial U}{\partial X}\right)^2 + \left(\frac{\partial V}{\partial Y}\right)^2 \right) + \left(\frac{\partial U}{\partial Y} + \frac{\partial V}{\partial X}\right)^2 \right] \end{aligned}$$

where ϕ is the irreversibility ratio, defined as

$$\phi = \frac{\mu T_0}{k} \left(\frac{\alpha}{L \Delta T}\right)^2$$

μ and k being dynamic viscosity and thermal conductivity of the fluid respectively. Here, we have considered ϕ as 10^{-4}.
The local entropy generation S_l is the sum of S_θ and S_ψ:

$$S_l = \left[\left(\frac{\partial \theta}{\partial X}\right)^2 + \left(\frac{\partial \theta}{\partial Y}\right)^2 \right] + \phi \left[2 \left(\left(\frac{\partial U}{\partial X}\right)^2 + \left(\frac{\partial V}{\partial Y}\right)^2 \right) + \left(\frac{\partial U}{\partial Y} + \frac{\partial V}{\partial X}\right)^2 \right]$$

The total entropy generation due to heat transfer to ($S_{t\theta}$) and due to fluid friction $S_{t\psi}$ are obtained by integrating the local entropy generation by the system volume

$$S_{t\theta} = \int_V S_\theta dV$$
$$S_{t\psi} = \int_V S_\psi dV$$
$$S_{total} = S_{t\theta} + S_{t\psi}$$

The average Bejan number indicates the strength of the entropy generation due to heat transfer irreversibility and is defined as the ratio of heat transfer irreversibility to total entropy generation

$$Be_{avg} = \frac{S_{t\theta}}{S_{t\theta} + S_{t\psi}} = \frac{S_{t\theta}}{S_{total}}$$

If $Be_{avg} > \frac{1}{2}$, the heat transfer irreversibility is dominating, while if $Be_{avg} < \frac{1}{2}$, the irreversibility due to fluid friction dominates the process and if $Be_{avg} = \frac{1}{2}$, the entropy generation due to viscous effects and heat transfer are equal.

3.5 *Heat function*

The heatline can be used to visualize the path line and intensity of heat flow which is similar to streamlines. The heatflow within the enclosure is displayed by using the heat function Π obtained from conductive heat fluxes $\left(-\frac{\partial\theta}{\partial X}, -\frac{\partial\theta}{\partial Y}\right)$ as well as convective heat fluxes $(U\theta, V\theta)$. The dimensionless form of heat function for a two dimensional convective problem can be obtained from

$$\frac{\partial\Pi}{\partial Y} = U\theta - \frac{\partial\theta}{\partial X}$$
$$-\frac{\partial\Pi}{\partial X} = V\theta - \frac{\partial\theta}{\partial Y}$$

which are derived from eqs. (1) and (4).

The above eqs. lead to the following differential equation for heat function

$$\frac{\partial^2\Pi}{\partial X^2} + \frac{\partial^2\Pi}{\partial Y^2} = \frac{\partial}{\partial Y}(U\theta) - \frac{\partial}{\partial X}(V\theta) \tag{7}$$

where Π is dimensionless heat function. We consider that Π is a continuous function with continuous second order partial derivatives. It should be noted that the positive sign of

Π denotes counterclockwise circulation and negative sign denotes clockwise heat flow.
The boundary conditions for Π are specified as follows:
At bottom wall, $n.\nabla\Pi = 0$,
At left wall, $n.\nabla\Pi = 1$,
At right wall, $n.\nabla\Pi = -1$,
At top curved wall, $\Pi = 0$

The following Dirichlet's conditions are used:
At bottom left corner $\Pi = \overline{Nu_l}$,
At bottom right corner $\Pi = -\overline{Nu_r}$
where $\overline{Nu_l}$ and $\overline{Nu_r}$ are average Nusselt number at left and right wall respectively.

4 Numerical Procedure

Eliminating the pressure term from eq.(2) and (3) and rewriting the equation of conservation of mass, momentum in terms of stream function (ψ) and vorticity (ω), we get

$$\frac{\partial^2\psi}{\partial X^2} + \frac{\partial^2\psi}{\partial Y^2} = -\omega, \tag{8}$$

$$Pr\left(\frac{\partial^2\omega}{\partial X^2} + \frac{\partial^2\omega}{\partial Y^2}\right) - \left(U\frac{\partial\omega}{\partial X} + V\frac{\partial\omega}{\partial Y}\right) + RaPr\frac{\partial\theta}{\partial X} = 0, \tag{9}$$

where

$$U = \frac{\partial\psi}{\partial Y}, \quad V = -\frac{\partial\psi}{\partial X}.$$

The irregular physical domain (X, Y) is transformed and converted into a regular (square) computational domain using coordinate transformation

$$\xi = X \qquad \eta = Y/(1 + hsin\pi X)$$

The above transformation transforms the curved upper boundary $Y = F(X)$ into the straight line $\eta = 1$.
The equations can be evaluated in $\xi - \eta$ domain using the following relationship

$$\begin{pmatrix} \frac{\partial\xi}{\partial X} & \frac{\partial\xi}{\partial Y} \\ \frac{\partial\eta}{\partial X} & \frac{\partial\eta}{\partial Y} \end{pmatrix} = \frac{1}{J}\begin{pmatrix} \frac{\partial Y}{\partial\eta} & -\frac{\partial X}{\partial\eta} \\ -\frac{\partial Y}{\partial\xi} & \frac{\partial X}{\partial\xi} \end{pmatrix}$$

where,

$$J = \frac{\partial(X,Y)}{\partial(\xi,\eta)} = \begin{vmatrix} \frac{\partial X}{\partial \xi} & -\frac{\partial X}{\partial \eta} \\ -\frac{\partial Y}{\partial \xi} & \frac{\partial Y}{\partial \eta} \end{vmatrix}.$$

It is difficult to solve the problem analytically due to the existence of non-linear terms in the governing Eqs. (1-4). Using the aforesaid transformation, the equations are changed into a bi-harmonic equation in the stream function-velocity formulation.The transformed equations are discretized using a finite difference scheme. An outer-inner iteration procedure, biconjugate gradient stabilized method (BiCGStab) is used to solve the discretized stream function ψ equation. The tri diagonal system

$$\left(\frac{\partial \psi}{\partial \xi}\right)_{i+1,j} + 4\left(\frac{\partial \psi}{\partial \xi}\right)_{i,j} + \left(\frac{\partial \psi}{\partial \xi}\right)_{i-1,j} = \frac{3}{d}(\psi_{i+1,j} - \psi_{i-1,j}), \quad (10)$$

$$\left(\frac{\partial \psi}{\partial \eta}\right)_{i,j+1} + 4\left(\frac{\partial \psi}{\partial \eta}\right)_{i,j} + \left(\frac{\partial \psi}{\partial \eta}\right)_{i,j-1} = \frac{3}{d}(\psi_{i,j+1} - \psi_{i,j-1}). \quad (11)$$

where d is the step length on a uniform rectangular mesh, is solved by using Thomas algorithm to get ψ_ξ and ψ_η. The computed ψ_ξ and ψ_η values are then used to derive velocity values, u^* and v^*. More details of the used numerical scheme are presented in [25]. The numerical method was implemented in FORTRAN-95 software. The cycle of numerical iteration continues until the convergence criterion (0.5×10^{-6}) is satisfied. The graphical presentation of this study has been performed by using GNUPLOT.

5 Results and discussion

In this section, numerical studies of flow and heat transfer in a complex enclosure are discussed. Computations are carried out for various Rayleigh number ($Ra = 10^3 - 10^5$), Prandtl number ($Pr = 0.7$ and 1000) with various amplitude (h) of top wall. Five different shapes of top wall are considered in order to emphasize the curvature effect on fluid flow and heat flow distribution. The original unit square enclosure is modified into a complex enclosure by changing the curvature of the top wall. Figs. 3-6 represent the isotherms (θ),streamlines (ψ), entropy generation due to heat transfer (S_θ), entropy generation due to fluid friction (S_ψ) and heatlines (Π) for different values Pr, Ra and h.

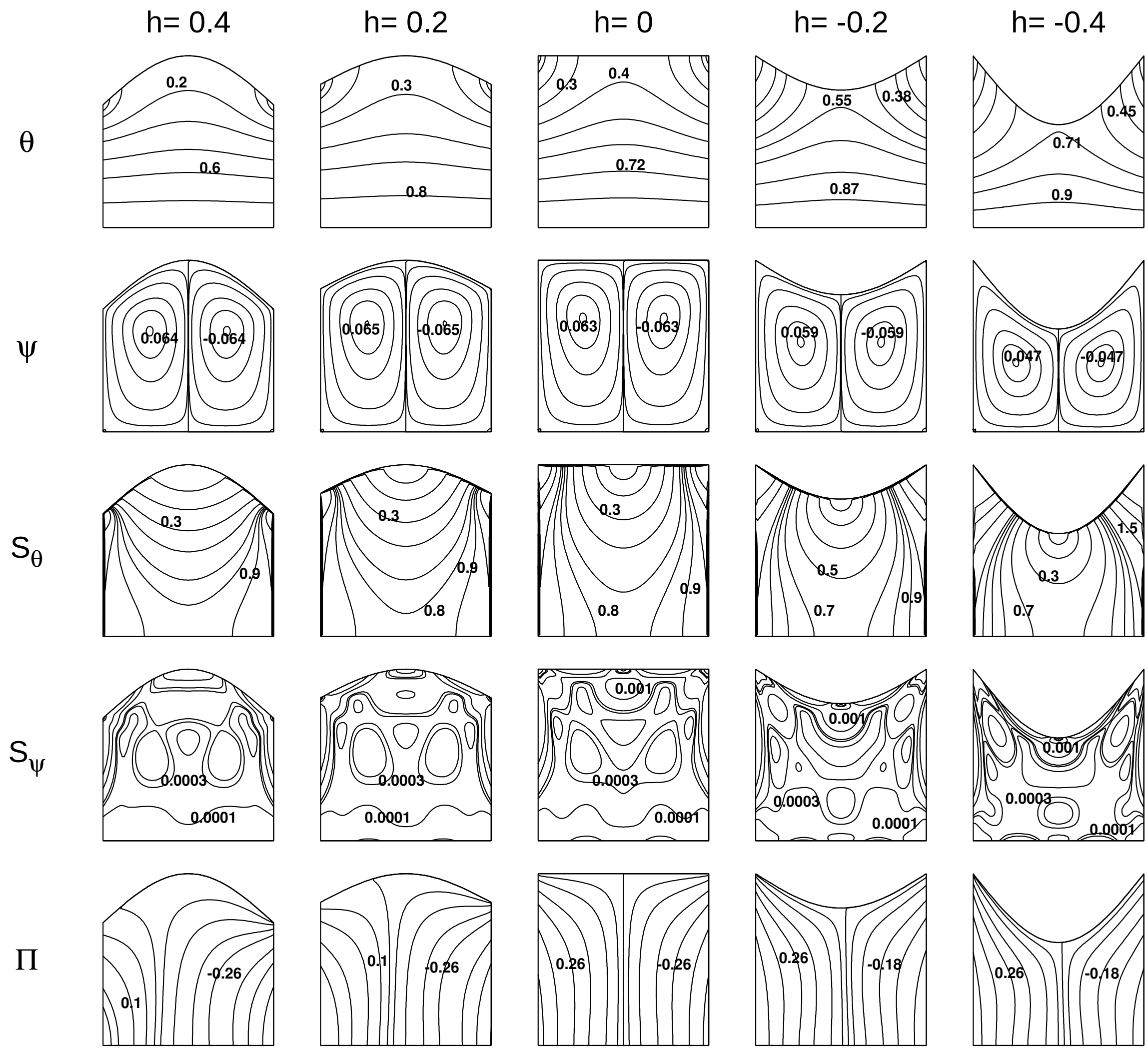

Fig. 2: Isotherms (θ), streamlines (ψ), entropy generation due to heat transfer (S_θ), entropy generation due to fluid friction (S_ψ) and heatlines (Π) for $Pr = 0.7$ and $Ra = 10^3$.

5.1 Streamlines and isotherms

It is clear from Fig. 2 that at low $Ra = 10^3$ the buoyancy effect is weak and heat transfer is primarily due to conduction. Isotherm lines are smooth, uniform and parallel near the uniformly heated bottom wall and follow the geometry of wavy surface. For square enclosures ($h = 0$), isotherms with $\theta \geq 0.4$ are smooth curves which span the entire enclosure and with $\theta \leq 0.3$, the isotherms occur symmetrically near the top corners of the linearly heated side walls. As the concavity increases, the qualitative trends of isotherms remains almost similar to square enclosure while as convexity increases the isotherms are found to be compressed at the corner regions due to less availability of area signifying higher heat transfer rate. The fluid near the bottom wall is hotter and have lower density. As a result, the fluid moves upward from the middle portion of the bottom wall towards the crest of the cavity and falls along the side walls forming two symmetric counter-rotating circulations having the same strength with respect to the centerline of the cavity. As Ra is low, the circulation is weak due to less prominent convection (see Fig. 2). It is found that $|\psi|_{max} = 0.063$ for square enclosure. As the concavity of the top wall increases, slight increase in the magnitude of $|\psi|_{max}$ is observed which in contrast significantly decreases as the convexity increases.

As Ra increases to 10^4, the isothermal lines swirl due to the influence of convection current for all h (Fig. 3). Also the buoyancy effect increases which results in expansion of vortices and becomes dense. The intensity of fluid flow increases to $|\psi|_{max} = 1.69$ for $h = 0$ as compared to the case of $Ra = 10^3$. Further $|\psi|_{max}$ increases or decreases on increasing the concavity and convexity respectively (Fig. 3).

Beyond $Ra = 10^4$, the effect of viscous force becomes weak and thermal force plays a dominant role. Significant distortion of the isotherms occur within the enclosures because of high convection. Largely compressed isotherms are observed near the side walls and middle portion of the square enclosure. Thermal boundary layers are observed near the vicinity of the bottom wall. On increasing concavity isotherms are found to be highly dispersed whereas highly compressed isotherms are observed as the convexity increases enhancing higher heat transfer rate. In other words, the heat transfer is dominated by convection rather than conduction under high Ra. Multiple circulations are observed in square enclosure with greater magnitude $|\psi|_{max} = 6.6$ at $Ra = 10^5$. Due to enhanced buoyant force, the intense primary circulations fill the upper portion of the enclosure and the lower portion is filled by secondary circulations. As h increases the intensity of primary as well as secondary circulation increases. In the reverse scenario the multicellular flow patterns turns into a bicellular flow pattern with the increase of convexity. (Fig. 4). Due to high momentum diffusivity at high $Pr = 1000$ and $Ra = 10^5$, the isotherms get further compressed along the lower and side wall in square enclosure (Fig. 5). On increasing concavity of the top wall, the isotherms starts getting deformed because of enhanced convection. As the buoyancy force starts dominating the viscous force at high Ra and hence the isotherms are unable to maintain the smoothness and dispersed throughout the enclosure. Significantly stronger intensity of fluid circulations can be seen from Fig. 5 which shows $|\psi|_{max} = 11.1$ for square enclosure. The increase in magnitude of $|\psi|_{max}$ illustrates that convection strength increases with high Pr. The primary fluid circulation vortices grow bigger in size and occupy almost the entire part of the enclosure. However, the secondary vortices are found near the corners of the bottom wall. It is also observed that the fluid takes the shape of the cavity for higher Pr that signifies thermal mixing. Reasonable changes are observed on increasing concavity of top wall. The two symmetric primary vortices in square enclosure splits into multiple vortex, one large dominated vortex diagonally elongated and secondary vortices appear above and below the diagonal vortex (Fig. 5). The two inner vortices are merged with each other in an elongated vortex. On increasing the convexity of the top wall, the secondary circulations are squeezed and begin to disappear and symmetric eddies are observed with decrease in magnitude of $|\psi|_{max}$ because of high convection effect.

5.2 Entropy generation

Entropy generation is due to two factors, heat transfer irreversibility (S_θ) and fluid friction irreversibility (S_ψ). At $Pr = 0.7$ and low $Ra = 10^3$, it is observed that the value of entropy generation due to fluid friction is negligible with respect to entropy generation due to heat transfer. Fig. 2 shows that due to high thermal gradient between the top wall and side wall, the maximum value of S_θ ($S_{\theta,max} = 17.42$) occurs at the top corners for square enclosure. The values of S_θ are very low at the central zone of the enclosure due to low temperature gradient. As h increases from zero to positive values the isotherms get

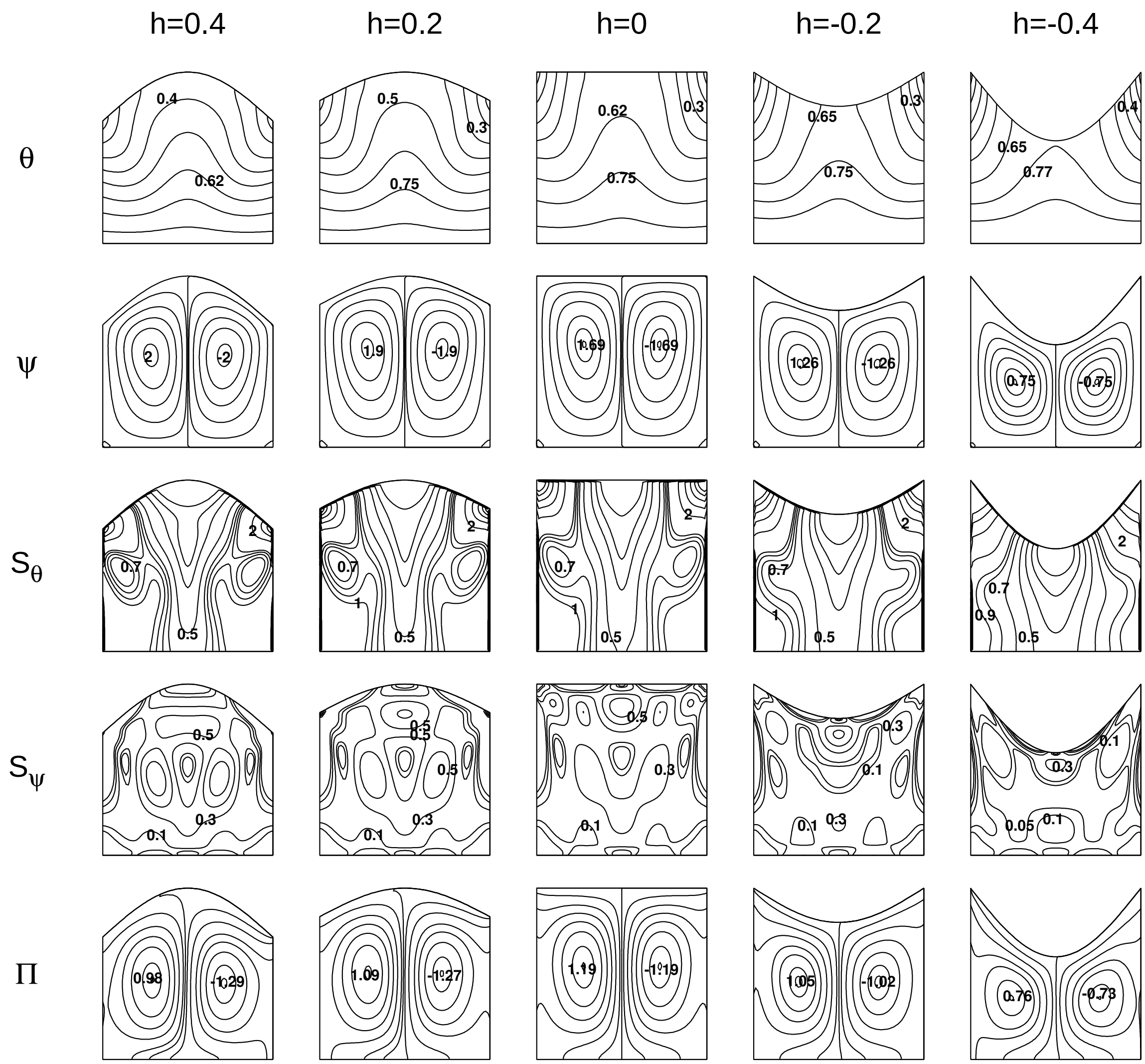

Fig. 3: Isotherms (θ), streamlines (ψ), entropy generation due to heat transfer (S_θ), entropy generation due to fluid friction (S_ψ) and heatlines (Π) for $Pr = 0.7$ and $Ra = 10^4$.

dispersed resulting in less thermal gradient and the value of $S_{\theta,max}$ decreases, whereas when h decreases from zero, largely compressed isotherms are observed near the side and top wall which results in increasing temperature gradient and consequently $S_{\theta,max}$ increases (see Table 3). Table 4 shows the maximum values of S_ψ for various values of Pr, Ra and h. It is clear from this table that as the fluid circulation cells are weak at low Ra, thus S_ψ is insignificant relative to S_θ with $S_{\psi,max} = 0.008$ for square enclosure. From Fig. 3 it is observed that the effect of S_ψ is significant at the corners of the curved wall of the enclosure because of velocity gradient between the cavity wall and adjacent flow circulation cell, while S_ψ is almost negligible at the core. Thus at low Ra, S_θ dominates S_ψ for all cases.

As Ra increases to 10^4, isotherms are found to be highly compressed due to enhanced convection, resulting in large $S_{\theta,max} = 25.29$ compared to the case of $Ra = 10^3$ for square enclosure (Fig. 3). As concavity increases more circular loops are observed due to which the heat transfer and $S_{\theta,max}$ decreases. Further it is observed that as convexity increases the circular loops dissolve indicating higher $S_{\theta,max}$ at the corner regions of the curved wall. Also high $S_{\psi,max} = 3.87$ for $h = 0$ is noticed because of increase in fluid flow and large velocity gradient. From Table 4, it can be seen that the convex cases exhibit lesser $S_{\psi,max}$ as compared to concave cases.

S_θ is significant for $Ra = 10^5$ due to high convection effect. Large compression of isotherms results in large $S_{\theta,max} = 43.92$ for square enclosure (see Fig. 4). The contours of S_θ at the core region are similar for all the cases ($S_\theta = 0.1$) due to less temperature gradient in this region. Because of high intensity of fluid circulation at $Ra = 10^5$, the velocity gradient are larger compared to temperature gradient resulting in larger $S_{\psi,max}$ for all h, see Table 4. An increase in concavity improves buoyancy and consequently the fluid flow effect which results in high S_ψ. Overall, it is observed that due to the presence of high convective effect at high Ra, the velocity gradient increases. Thus S_ψ dominates over S_θ throughout the cavity for all cases.

Maximum entropy generation due to heat transfer is observed for $Pr = 1000$ and $Ra = 10^5$ because of high temperature gradient. The isotherms are found to be strongly compressed as compared to $Pr = 0.7$ (Fig. 6). It is obtained that $S_{\theta,max} = 80.21$ for square enclosure. Strong convection induces greater buoyancy effect for high Pr . Similar to lower Pr, the value of $S_{\theta,max}$ for concave cases are less as compared to the convex cases due to highly compressed isotherms at the corner regions of the curved walls. Also the value of $S_{\psi,max}$ are larger for concave cases than those of convex cases (Table 4). The presence of intense streamline cells at $h = 0.2$ results in high velocity gradients causing higher value of $S_{\psi,max}$. S_ψ is almost similar at the interior region for all the cases. Comparatively larger values of $S_{\psi,max}$ are observed than those of $S_{\theta,max}$ throughout the enclosure.

Table 1: Values of $S_{\theta,max}$ at $Pr = 0.7$ and 1000 for $Ra = 10^3 - 10^5$ with various amplitude of upper wall (h).

	$Pr = 0.7$			$Pr = 1000$		
h	$Ra = 10^3$	$Ra = 10^4$	$Ra = 10^5$	$Ra = 10^3$	$Ra = 10^4$	$Ra = 10^5$
-0.4	64.58	69.63	101.65	64.58	69.54	109.03
-0.2	33.27	40.36	66.35	33.27	31.52	85.75
0	17.42	25.29	43.92	17.42	25.71	80.21
0.2	12.00	19.06	39.72	12.00	22.12	74.52
0.4	11.23	16.69	34.05	11.23	17.87	49.14

Table 2: Values of $S_{\theta,max}$ at $Pr = 0.7$ and 1000 for $Ra = 10^3 - 10^5$ with various amplitude of upper wall (h).

	$Pr = 0.7$			$Pr = 1000$		
h	$Ra = 10^3$	$Ra = 10^4$	$Ra = 10^5$	$Ra = 10^3$	$Ra = 10^4$	$Ra = 10^5$
-0.4	0.0076	1.39	237.55	0.0069	1.29	202.20
-0.2	0.0074	2.45	251.19	0.0073	2.83	291.84
0	0.0088	3.87	191.24	0.0071	3.54	359.82
0.2	0.0069	4.79	210.55	0.0072	4.19	375.30
0.4	0.0035	4.99	202	0.0077	5.74	296.18

5.3 Heatlines

The direction of heat flow is represented by heatlines. At low Ra, end to end heatlines connecting bottom wall and adjacent side walls are observed in Fig. 2. In this figure heatlines are smooth and symmetrical with respect to middle line for square enclosure

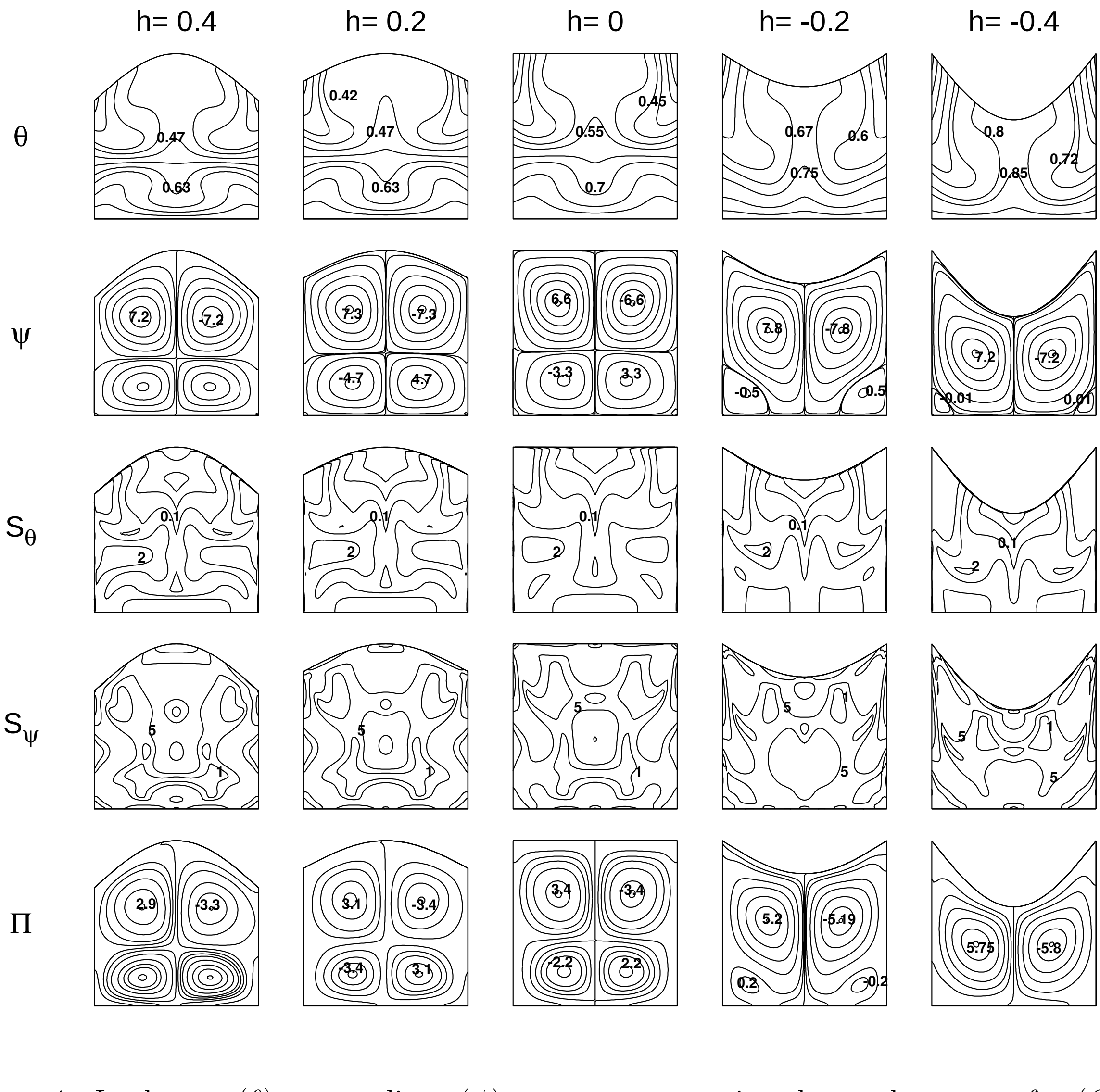

Fig. 4: Isotherms (θ), streamlines (ψ), entropy generation due to heat transfer (S_θ), entropy generation due to fluid friction (S_ψ) and heatlines (Π) for $Pr = 0.7$ and $Ra = 10^5$.

depicting high conductive heat transfer. Intense heatlines are occurred at the top portion of the side walls. It is noted that $|\Pi|_{max} = 0.46$ for $h = 0$ (Fig. 2). As the concavity increases, asymmetric heatlines are observed which are dense in upper portion of the right wall as compared to left wall and hence the value of $|\Pi|_{max}$ decreases. Whereas, on increasing convexity dense heatlines are observe at the upper portion of left wall as compared to right wall which results in increase in $|\Pi|_{max}$.

Interesting features are observed for $Ra = 10^4$ in Fig. 3. The straight heatlines are transformed to two symmetric eddies in the whole region of the enclosure due to convection dominant heat transfer. Intense vertical heatlines are observed at the core and near the side walls (Fig. 3). Similar to low Ra dense heatlines are formed in the right wall as h increases and in left wall as h decreases.

As $Ra = 10^5$, similar to streamline, symmetric primary heatline circulations are observed in the top portion and secondary circulations span near the lower half. Due to enhanced thermal mixing, higher intensity of closed loop heatlines are observed at the core. With the increase of Ra magnitude of heatfunction increases which implies that the amount of heat transfer rate is higher. The intensity of primary circulations are higher as compared to lower secondary circulations. As h decreases from 0 to -0.4, the secondary circulations begin to vanish and large symmetric primary circulations are found to span and take the shape of the enclosure. As a result heatlines are closely compact depicting higher heat transfer gradient. However as h increase from 0 to 0.4, intensity of primary circulation decreases and secondary circulation increases (Fig. 4).

For high $Pr = 1000$, $Ra = 10^5$, due to enhanced thermal mixing, two symmetric primary eddies are observed in square enclosure of high intensity and compressed secondary circulations of lower intensity near the bottom wall are formed. Magnitude of $|\Pi|_{max}$ is larger compared to low $Pr = 0.7$. As the concavity increases, the secondary eddies start to grow and at $h = 0.4$ large diagonally elongated eddies are formed having secondary eddies above and below the elongated eddies. While the secondary eddies begin to vanish as h decreases. (see Fig. 5)

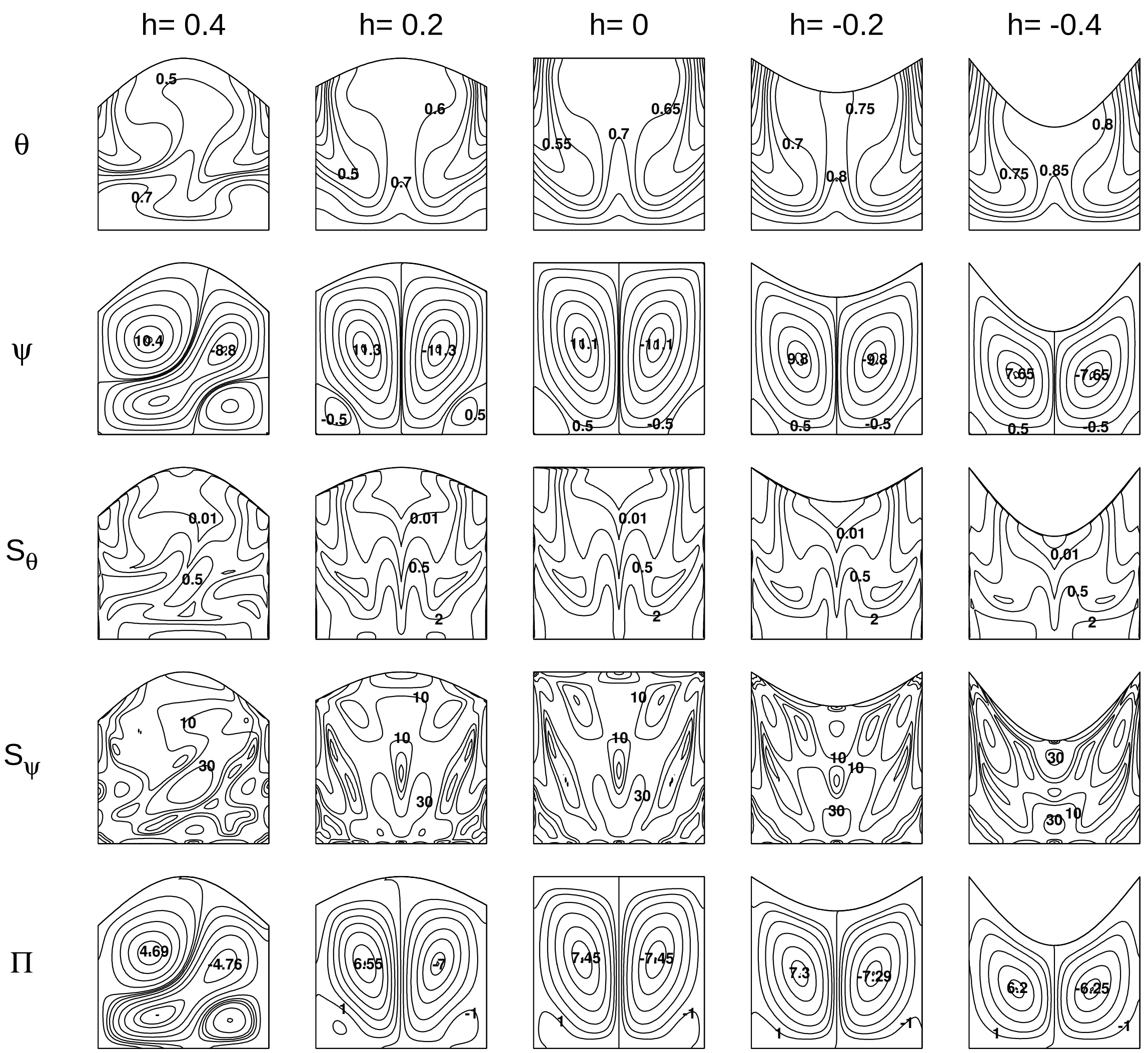

Fig. 5: Isotherms (θ), streamlines (ψ), entropy generation due to heat transfer (S_θ), entropy generation due to fluid friction (S_ψ) and heatlines (Π) for $Pr = 1000$ and $Ra = 10^5$.

5.4 Nusselt number and Bejan's number

Fig. 6 shows the effect of various curvature of the upper wall on average Nusselt number ($\overline{Nu}$) and average Bejan's number (Be_{avg}) for different Rayleigh number ($10^3 - 10^5$) at $Pr = 0.7$ and 1000.

Heat transfer is mainly due to conduction at low $Ra = 10^3$. As the convective mode of heat transfer becomes dominant with the increase of Ra, there is an increase in $\overline{Nu}$ for all values of h causing a high heat transfer effect within the enclosure. It is clear from Fig. 7 ((a) and (c)), the rate of heat transfer increases as h decreases when Ra and Pr are kept fixed. The $\overline{Nu}$ even becomes negative for $h = 0.4$ depicting that the heat generated in the bottom wall cannot be transferred to the top wall. This shows that $\overline{Nu}$ is larger in highly convex case ($h = -0.4$) as compared to other cases. Similar trend is observed at high $Pr = 1000$. Because of large momentum diffusivity at high Pr, $\overline{Nu}$ is significantly larger than that of $Pr = 0.7$ for all h.

At low $Ra = 10^3$, $Be_{avg} \cong 1$ for all values of h, because entropy generation due to heat transfer irreversibility is high compared to irreversibility effect caused by the fluid friction. As Ra increases, convection heat transfer becomes dominant, the effect of viscosity flow on entropy generation becomes stronger that leads to decrease in Be_{avg}. As h increases from 0 to 0.4, $S_{\theta,max}$ is larger than $S_{\psi,max}$ at $Ra = 10^3$. Whereas, as h decreases from 0 to -0.4 compressed isotherms are observed that results in increase in $S_{\theta,max}$ at $Ra = 10^5$ and consequently Be_{avg} increases (Fig. 6 ((b) and (d))). As Pr increases from 0.7 to 1000, Be_{avg} decreases due to high momentum diffusivity and rapid increase in magnitude of $S_{\psi,max}$ for all cases. Qualitative distribution of $\overline{Nu}$ and Be_{avg} are similar for $Pr = 0.7$ and 1000.

Overall it is observed that $Be_{avg} > \frac{1}{2}$ for low Ra which shows that heat transfer irreversibility is dominant in the enclosure while for high Ra, $Be_{avg} < \frac{1}{2}$ depicting that heat transfer irreversibility due to fluid friction becomes dominant.

6 Conclusion

Study of natural convection in a complex enclosure has been investigated numerically. The unit square enclosure is modified into a complex enclosure by changing the amplitude of

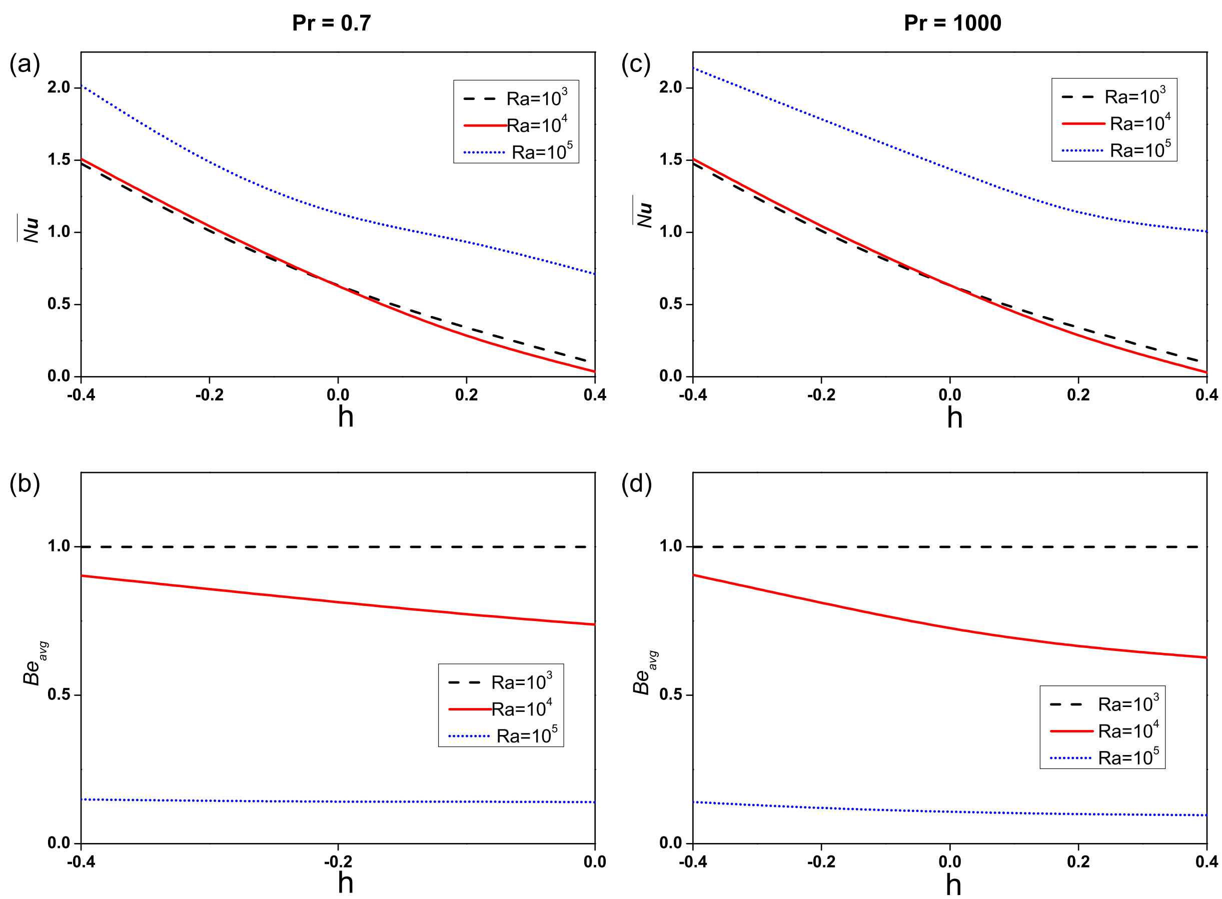

Fig. 6: Variation of average Nusselt number ($\overline{Nu}$) and average Bejan number (Be_{avg}) with h for various curvature at $Pr = 0.7$ and 1000.

the top curved wall. The thermal flow characteristics are obtained for various Rayleigh number ($10^3 - 10^5$) and $Pr = 0.7$ and 1000. The main conclusions drawn from the present study are as follows:

1. At low Ra heat transfer is due to conduction hence smooth isotherms are observed. The isotherms gets more compressed with the increase of Ra and Pr due to enhanced convection. Heat transfer rate is found to be more in convex cases as compared to concave cases.

2. The magnitude of $|\psi|_{max}$ is less at low Ra. The intensity and magnitude of streamlines increases with the increase of Ra and Pr. Multiple vortices are observed at $Ra = 10^5$. $|\psi|_{max}$ increases with the increase of h and decreases with the decrease of h.

3. $S_{\theta,max}$ increases with increase of Ra and Pr due to enhanced convection. Comparative studies show that $S_{\theta,max}$ is highest in convex cases and least in concave cases or all Ra and Pr.

4. $S_{\psi,max}$ is found to be very less at low Ra, which increases with the increase of Ra and Pr. As the fluid flow effect improves with increasing h, $S_{\psi,max}$ is found to be more in concave cases compared to convex cases.

5. Heatline contours are almost similar to streamlines. The intensity of heatline increases with the increase of Ra and Pr because of increase of convection. Dense heatlines are observed with the increase of h resulting in high magnitude of heatfunction whereas heatlines are found to be segregated as h decreases and the magnitude of heatfunction decreases.

6. $\overline{Nu}$ increase with the increase of Ra and Pr. As the heat transfer rate is found to be higher in convex cases as compared to concave cases, $\overline{Nu}$ increases when h decreases from 0 to -0.4 and decreases when h increases from 0 to 0.4.

7. At low Ra, $Be_{avg} > \frac{1}{2}$ which signifies that entropy generation in the enclosure is mainly due to heat transfer irreversibility. With the increase of Ra, buoyancy force becomes dominant which results in increase in entropy generation due to fluid friction irreversibility, consequently $Be_{avg} < \frac{1}{2}$.

References

[1] G.de Vahl Davis, Natural convection of air in a square cavity: a benchmark numerical solution, Int. J. Numerical Methods in fluids 3 (1983) 249-264.

[2] Q.H.Deng, G.F.Tang, Numerical visualization of mass and heat transport for conjugate natural convection/heat conduction by streamline and heatline, Int. J. Heat Mass Transfer 45 (2002) 2373-2385.

[3] T.Basak, S. Roy, A.R. Balakrishnan Effects of thermal boundary conditions on natural convection flows within a square cavity, Int. J. Heat Mass Transfer 49 (2006) 4525-4535.

[4] S.Kimura, A.Bejan, The Heatline visualization of convective heat transfer, J. Heat Transfer 105 (1983) 916-919.

[5] S.C.Saha, M.M.K.Khan, A review of natural convection and heat transfer in attic-shaped space, Energy and Buildings 43 (2011) 2564-2571.

[6] E.Faud Kent, Numerical analysis of laminar natural convection in isosceles triangular enclosure for cold base and hot inclined walls, Mechanics Research Comm. 36 (2009) 497-508.

[7] E.Faud Kent, E. Asmaz, S. Ozerbay, Laminar natural convection in right triangular enclosures, Heat Mass Transfer 44 (2007) 187-200.

[8] O.Aydin, A. Unal, T. Ayhan, Natural convection in rectangular enclosures heated from one side and cooled from the ceiling, Int. J. Heat Mass Transfer 42 (1999) 2345-2355.

[9] G.G.Ilis, M.Mobedi, B. Sunden, Effect of aspect ratio on entropy generation in a rectangular cavity with differentially heated vertical walls, Int. comm. in Heat Mass transfer 35 (2008) 696-703.

[10] F.Moukalled, M.Darwish, Natural convection in a trapezoidal enclosure heated from the side with a baffle mounted on its upper inclined surface, Heat Tranfer Engg. 25 (8) (2004) 80-93.

[11] D.Ramakrishna, T.Basak, S. Roy, Analysis of heatlines and entropy generation during free convection within trapezoidal cavities. Int. Comm. in Heat Mass Transfer 45 (2013) 32-40.

[12] T.Basak, P.Kumar, R. Anandalakshmi, S. Roy, Analysis of Entropy Generation Minimization during Natural Convection in Trapezoidal Enclosures of Varoius Angles with Linearly Heated Side Wall(s), Industrial and Engg. Chem. Research 51 (2012) 4069-4089.

[13] R.Anandalakshmi, T.Basak, Heat flow visualization for natural convection in rhombic enclosure due to isothermal and non-isothermal heating at the bottom wall, Int. J. Heat Mass Transfer 55 (2012) 1325-1342.

[14] Y.S.Morsi, S.Das, Numerical Investigation of Natural Convection inside Complex Enclosures, Heat Transfer Engg. 24 (2) (2003) 30-41.

[15] S.Abdelkader, R.Mebrouk, B. Abdellah, B. Khadidja, Natural convection in a Horizontal Wavy Enclosure, J. of Applied Sciences 7(3) (2007) 334-341.

[16] Y.Varol, H.F.Oztop, Buoyancy induced heat transfer and fluid flow inside a tilted wavy solar collector, Building and Environment 42 (2007), 2062-2071.

[17] P.K.Das, S.Mahmud, Numerical investigation of natural convection inside a wavy enclosure, Int. J. Therm. Sci. 42 (2003) 397-406.

[18] S.Mahmud, A.K.M.Sadrul Islam, Laminar free convection and entropy generation inside an inclined wavy enclosure, Int. J. Therm. Sci. 42 (2003) 1003-1012.

[19] A.Dalal, M.K.Das, Natural Convection in a Cavity With a Wavy Wall Heated From Below and Uniformly Cooled From the Top and Both Sides, J. of Heat Transfer 128 (7) (2006) 717-725.

[20] A.Dalal, M.K.Das, Heatline method of visualization of natural convection in a complicated cavity, Int. J. Heat Mass Transfer 5 1(2008) 263-272.

[21] L.Adjoult, O. Imine, A. Azzi, M. Belkadi, Laminar natural convection in an inclined cavity with a wavy wall, Int. J. Heat Mass Transfer 45 (2002) 2141-2152.

[22] A.Misirlioglu, A.C.Baytas, I. Pop, Free convection in a wavy cavity filled with a porous medium, Int. J. Heat Mass Tranfer 48 (2005) 1840-1850.

[23] P.Biswal, T.Basak, Entropy generation based approach on ntural convection in enclosure with concave/convex side walls, Int. J. Heat Mass Transfer 82 (2015) 213-235.

[24] P. Biswal, T. Basak, Bejan's heatlines and numerical vizualization of convective heat flow in flow in differentially heated enclosure with concave/convex side walls, Energy 64 (2014) 69-94.

[25] R. Parveen, T.R. Mahapatra, Numerical simulation of MHD double diffusive natural convection and entropy generation in a wavy enclosure filled with nanofluid with discrete heating, Heliyon 5 (2019) e02496.

[26] Q.H.Deng, G.F.Tang, Numerical visualization of mass and heat transport for conjugate natural convection/heat conduction by streamline and heatline, Int. J. Heat Mass Transfer 45 (2002) 2373-2385.